Capillarity

Original article

Water uptake in parallel fractures

Junjie Wang[1], Xingyu Zhu[2], Yixin Pan[1]*, Jisheng Kou[1], Shuyu Sun[2]

[1]*Key Laboratory of Rock Mechanics and Geohazards of Zhejiang Province, Shaoxing 312000, P. R. China*
[2]*Computational Transport Phenomena Laboratory, Division of Physical Science and Engineering, King Abdullah University of Science and Technology, Thuwal 23955-6900, Kingdom of Saudi Arabia*

Abstract:
Water uptake in rock fractures caused by rainfall plays a significant role in slope stability analysis. Since the fracture network system has complicated structures and multiple scales, the models based on the averaged system cannot account for these properties. On the other hand, a model describing a single fracture with fractal characteristics and surface roughness fails to deal with the case of multiple fractures at spatial scales. In this study, a fracture-network model is established to account for the complex structures and multiple scales of fractures. By considering the connectivity between fractures and the limited area of aquifer, capillary pressure formulations in different fractures are derived based on the Young-Laplace equation, and the final water level under specific rainfall conditions is also obtained. The cross-section shapes and exhaust conditions of rainwater infiltration have important influences on the final water level. The results indicate that the final water level is proportional to the ratio of perimeter to cross-section area when the fracture is a cylinder, and a circular pipe can reduce water level elevation in the fracture system.

1. Introduction

Slope stability is significantly influenced by water uptake in ground material fractures caused by rainfall. Torrential rainfalls may cause landslides in mountain areas around the world, as rainwater infiltrates into the soil with an increasing content and pressure, which could weaken soil strength and stiffness (Terzaghi, 1950; Sidle and Swanston, 1982; Sitar et al., 1992; Anderson and Sitar, 1995; Wang and Sassa, 2003; Regmi et al., 2017). If the rain is a heavy torrential one, landslides and slope failures may take place (Brand, 1984; Brenner et al., 1985). Consequently, the permeation of water into the soil and the resulting pore pressure variation are crucial for understanding the transient conditions of slope failure (Lu and Godt, 2013; Cho, 2016).

Researches on rainfall infiltration into fractures must consider the morphology and distribution of these fractures. The theory of continuous media has been widely employed in this research topic, while rock and soil cannot be treated as a continuous medium due to the presence of discontinuity, anisotropy and inhomogeneity. These features give rise to

the difficulty of relevant theoretical research. In networked fractures, different fractures have their respective distinctive seepage parameters, and the fracture conjunctions are generally complex, thus it is hard to obtain theoretical results (Wang et al., 1998). Moreover, due to the complex fracture structure and undulation characteristics of the fracture surfaces, it is difficult to characterize the fracture morphology. The fractal dimensions of fracture surface morphology are within a certain scale range, which are not the theoretical fractal objects (Dong, 2020). On the other hand, the flow of fluid in the fractures also greatly impacts the fracture structures and commonly results in the change of morphology and distribution. However, the migration mechanism of water flow in fractures is still not fully understood (Zheng et al., 2019). In order to resolve the above problems, researchers have introduced many models to date. While a practical seepage model for fractured rock mass could describe the seepage mechanism of primary and secondary fracture systems in detail, the double fracture systems seepage principle provides a new method to analyze the seepage rock mass fractures in engineering (Wang et al., 1998). The fractal self-affinity rough fracture is taken into account in

another model, and the Cuckoo Search algorithm optimizes the segmentation of fracture surface, which can be used to study the roughness characteristics of fracture surface (Dong, 2020). The relationships among hydraulic gradient, flow rate and solute transport law were studied in a single marble parallel plate fracture (Zheng et al., 2019).

Although great progress has been made in the seepage theory of water in fractures, it is difficult to extend the existing theory to describe multiple fractures. In the theoretical calculation of the complete fracture network model, many specific parameters that never appear in single fractures are largely ignored. In this work, a fracture network system is established based on specific fracture morphology and distribution. Considering the connectivity between fractures and the limited area of the aquifer, capillary pressure under different fractures is derived based on the Young-Laplace equation, and the final water level under specific rainfall conditions is obtained. The influences of cross section shapes and exhaust conditions of rainwater infiltration on the final water level are studied to make the theory applicable to more diverse situations.

2. The influence of geometric features on water level changes

2.1 Model description

It is assumed that the bottom of the rock and the soil mass are impermeable boundaries, that is, water cannot penetrate into the impermeable layer below. There are a series of fractures within the rock and soil mass, which constitute a fracture system. The space of each fracture is a four-prism, which is perpendicular to the horizontal plane. The lateral interface between the fracture space and the rock is called fracture plane. Each fracture space has two pairs of parallel fracture planes, thus they are called parallel fractures. The shape of a parallel fracture is shown in Fig. 1.

The rock interlayer between fractures is impermeable, thus water in one fracture cannot penetrate into another fracture directly through the interlayer. Only the upper part of fractures is free surface, while the bottom part is connected to the aquifer that is always in contact with air. Water contained in the aquifer cannot drain.

When rainfall occurs, water infiltrates the fracture system resulting in the rise of water level, which in turn affects slope stability (Kristo et al., 2017). The final water level is studied under different conditions, including rainfall intensity, spatial
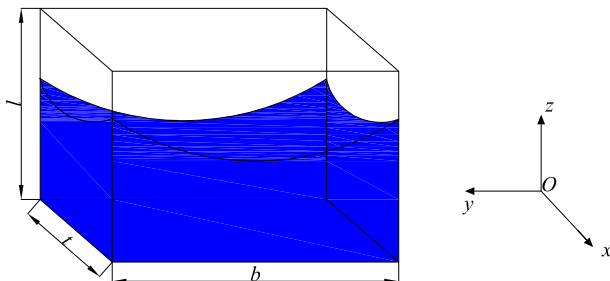

Fig. 1. Schematic diagram of each parallel fracture.

geometry (dimensions) of fractures, distribution forms of fractures, initial water level, density of liquid and gas phases, gravity, interfacial tension and wetting angle of liquid and gas phases. The influence of temperature change is neglected. The calculation of water level in fractures with different forms and distributions under specific rainfall conditions by considering capillary pressure has great geophysical significance. The characteristics of fractures of rock and soil mass are highly complex in nature, and the influence of the dynamic process of penetration on slope stability is a persistent problem that needs to be urgently solved.

2.2 Parallel and equal aperture vertical fractures

2.2.1 Bottom separation condition

Physical, chemical and biological processes influence different rock and soil masses that are formed under varying geological conditions. These influence factors are specifically reflected in the primary role of some geophysical processes including metamorphism, melt and solidification cycles, and plate movement, and in the secondary role of weathering (Nesbitt et al., 1982). The masses formed include sedimentary rocks, metamorphic rocks and magmatic rocks, which may develop different fissures (Dill, 2016).

In this paper, it is assumed that the fracture surface of the rock mass is continuous, isotropic, planar and vertically distributed, and the top surface of the rock and soil mass is horizontal. The inner surfaces of the fracture space are denoted as the fracture surfaces, and opposite surfaces are parallel to each other. The fractures are connected with the rest of the rock mass at the bottom. They are mutually separated and disconnected, and the interlayers between fractures are impermeable. The fracture system is connected to the precipitation area, and the water volume at the top of the impermeable layer is infinite compared to the pore cross-sectional area. Therefore, the increase of water level caused by pore pressure cannot lead to a decreased original water level. If the impermeable top surface is called base surface, a Cartesian coordinate system $x-y-z$, with the vertical direction as z and the base surface as $y-O-x$ surface, can be established. It is assumed that the fractures are hydrophilic, that is, water is the wetting phase while air is the non-wetting phase. In this case, the wetting angle is less than $90°$, and thus capillary pressure will provoke the rise of water in fractures. The fracture surface is simplified as a rectangle with length l (vertical length) and width b, and the fracture aperture is represented by t, the fracture thus forming a four-prism. Let the initial water level be z_0. Precipitation with a total volume of V enters the fracture system during investigation time ΔT, which has n equal large fractures. During this period, if capillarity pressure is neglected, the water level rise should be

$$\Delta z = \frac{V}{nbt} \tag{1}$$

where Δz is the variation of water level.

Consider the contribution of capillary pressure and assume that the free interface is a meniscus surface in the x direction and the y direction, i.e., the interface is 'Mouhe Square Cover',
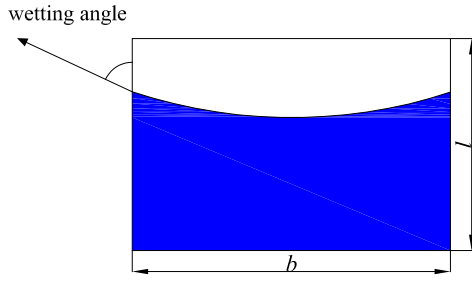
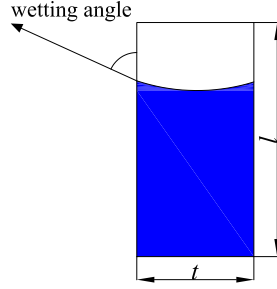**Fig. 2.** Surface tension of water-air interface on cross-section *bl*.

Fig. 3. Surface tension of water-air interface on cross-section *tl*.

which can be regarded as the intersecting surface of two cylindrical surfaces. Figs. 2 and 3 show the surface tension of the water-air interface in different directions.

Based on the geometric relationships

$$R_1 = \frac{b}{2\cos\theta} \tag{2}$$

$$R_2 = \frac{t}{2\cos\theta} \tag{3}$$

the Young-Laplace equation (Liu and Cao, 2016) gives the capillary pressure p_c of a single fracture:

$$p_c = 2\sigma\cos\theta\left(\frac{1}{b}+\frac{1}{t}\right) \tag{4}$$

where θ represents the wetting angle at the water-fracture interface, σ is the surface tension, b denotes the width of the fracture surface, and t represents the aperture of the fracture.

Eq. (4) is based on the Young-Laplace equation:

$$p_c = \sigma\left(\frac{1}{R_1}+\frac{1}{R_2}\right) \tag{5}$$

where R_1 and R_2 are the radii of curvature circle in the orthogonal direction of the interface.

Next, a simple force analysis is carried out for the process of water level rise. Before the occurrence of capillarity, the water content of the fracture system increases due to precipitation, and the water level consequently rises. The rising height is V/nbt, as shown in Eq. (1). Due to capillarity, the surface tension shows upward capillary pressure. The hydraulic pressure in the fracture is unbalanced, thus water transports upward. When the water level rises, the pore water pressure will increase, and the fluid level will keep moving

until the upward capillary pressure is equal to the downward gravity increment (neglecting the vibration process). When the system reaches an equilibrium state, the water head is denoted by z, and the actual height increment caused by capillary pressure is represented by $\Delta h'$, which satisfies

$$z = z_0 + \Delta z + \Delta h' \tag{6}$$

The expressions of the capillary force F and the gravity increment ΔG are now shown as

$$F = p_c bt = 2\sigma\cos\theta\left(\frac{1}{b}+\frac{1}{t}\right)bt \tag{7}$$

$$\Delta G = mg = (\rho_w - \rho_n)ghbt \tag{8}$$

where m is the mass increment of the matter in the fracture, ρ_n and ρ_w are non-wetting phase density and wetting phase density, respectively, and g denotes gravitational acceleration.

According to Newton's first law,

$$F = \Delta G \tag{9}$$

the water level height can be obtained as

$$h = \frac{2\sigma\cos\theta}{(\rho_w - \rho_n)g}\left(\frac{1}{b}+\frac{1}{t}\right) \tag{10}$$

which can be rewritten by multiplying the numerator and denominator by bt:

$$h = \frac{2\sigma\cos\theta(b+t)}{(\rho_w - \rho_n)gbt} \tag{11}$$

Eq. (11) is a different form of h, which will be discussed later.

Capillary pressure causes water level to rise. Accordingly, the water level in the aquifer slightly drops, and can be expressed as

$$S_{aqi}\Delta h = bt\Delta h' \tag{12}$$

where S_{aqi} represents the area of the aquifer exposed to the atmosphere (the area of the fracture excepted), Δh represents the decrease of the water level of the aquifer exposed to the atmosphere, and $\Delta h'$ represents the actual rise of the water level in the capillary. It can be obtained as

$$h = \Delta h + \Delta h' \tag{13}$$

Eqs. (12) and (13) can be combined, and the linear equation system with two unknown variables can be solved as follows

$$\Delta h = \frac{bth}{S_{aqi}+bt} \tag{14}$$

$$\Delta h' = h - \frac{bth}{S_{aqi}+bt} \tag{15}$$

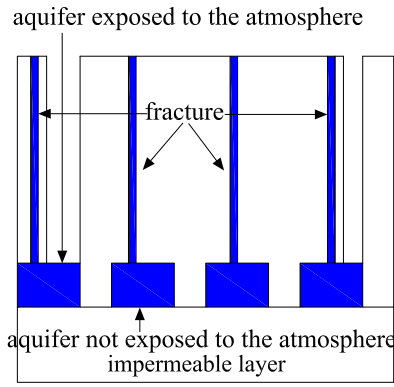It can be seen that $S_{aqi}+bt$ is the area of the water connected with air.

Fig. 4. Parallel equal aperture vertical separated fractures.

Fig. 6. Parallel and equal aperture vertical interconnected fractures.
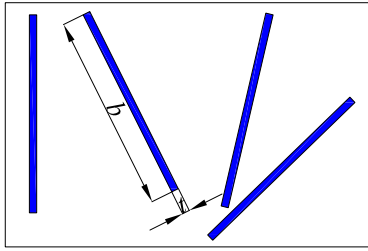

Fig. 5. Top view of fracture distribution in other cases.

Based on Eqs. (1), (6), (11) and (15), the following equation can be derived:

$$z = z_0 + \frac{V}{nbt} + \frac{2\sigma \cos(b+t)S_{aqi}}{(\rho_w - \rho_n)gbt(S_{aqi} + bt)} \tag{16}$$

Eq. (16) describes the final position of the water level of a single fracture under the condition of uniform precipitation. The capillary phenomenon appears only when the aquifer is exposed to air. Fig. 4 shows the parallel and equal aperture vertical separated fractures.

It should be noted that the distribution modes include, but are not limited to this condition. Fig. 5 shows one of the top views of other fracture distributions.

It is clear from Eq. (16) that the water level is related to the area of the aquifer exposed to air, the initial water level, precipitation, number of fractures, width and aperture of fractures, surface tension, wetting angle, and phase density. The increase of the aquifer area exposed to air, the initial water level, the precipitation, the surface tension, or the ratio of perimeter to area together determine the degree of final water level increase. Meanwhile, the increase of density difference between the two phases, the gravitational acceleration, or the cross sectional area of fracture influence the final water level decrease.

2.2.2 Bottom interconnection condition

In this section, the water level change under the interconnected condition of the fracture system (Ding et al., 2020) is considered. Fig. 6 illustrates the parallel and equal aperture vertical interconnected fractures.
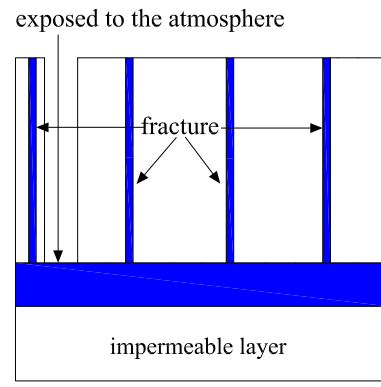
Compared to the change of water level of a system in which the fractures are disconnected, the change of water level in the connected case should take into consideration the influence of water pressure. The liquid that connects the fractures to each other as a communicator will eventually maintain the same level (Sasaki et al., 2006), however, this communicator principle is not applicable when the effect of capillary pressure is considered. It is assumed that there are two capillary pressures with different pore sizes, one of which rises to a higher level. In this case, the liquid slice method is used to carry out the force analysis, and it can be obtained as

$$p_{c1} + \rho_w gh_2 = \rho wgh_1 + p_{c2} \tag{17}$$

where h_1 and h_2 are the two liquid level heights related to the water, while p_{c1} and p_{c2} represent the corresponding capillary pressures. This can be rewritten as follows

$$p_{c1} - p_{c2} = \rho_w g(h_1 - h_2) \tag{18}$$

Based on the above formula, the capillary with higher capillary pressure has higher liquid level. That is, the communicator principle is not applicable and therefore cannot be applied for parallel fracture systems.

Based on the communicator principle of a capillary, we continue to derive the final liquid level height. By conducting the force analysis with the method of liquid slices, the following equations can be obtained:

$$p_{c1} = \rho_w gh_1 \tag{19}$$

$$p_{c2} = \rho_w gh_2 \tag{20}$$

Capillary pressure causes the water level to rise. Accordingly, the water level in the aquifer falls slightly, and can be obtained as

$$S_{aq}\Delta h = bt_1\Delta h_1 + bt_2\Delta h_2 \tag{21}$$

where S_{aq} represents the area of the aquifer exposed to the air (the fracture area excepted), Δh represents the decrease of the water level of the aquifer exposed to the atmosphere, Δh_1 represents the actual rise of water level in capillary 1, and Δh_2

represents the actual rise of water level in capillary 2. These can be obtained as

$$h_1 = \Delta h + \Delta h_1 \qquad (22)$$

$$h_2 = \Delta h + \Delta h_2 \qquad (23)$$

Eqs. (21), (22) and (23) can be combined and solved as follows

$$\Delta h = \frac{bt_1 h_1 + bt_2 h_2}{S_{aq} + bt_1 + bt_2} \qquad (24)$$

$$\Delta h_1 = h_1 - \frac{bt_1 h_1 + bt_2 h_2}{S_{aq} + bt_1 + bt_2} \qquad (25)$$

$$\Delta h_2 = h_2 - \frac{bt_1 h_1 + bt_2 h_2}{S_{aq} + bt_1 + bt_2} \qquad (26)$$

It can be seen that $S_{aq} + bt_1 + bt_2$ is the area of water connected to air.

Based on Eq. (11), it is obvious that if the aperture, width, the wetting angle and surface tension of each capillary are the same, equal water level rises can be obtained, such as

$$h_1 = h_2 \qquad (27)$$

Therefore, Δh, Δh_1, and Δh_2 will be also equal.

The above deduction can be extended to the case of n fractures. Under the condition of equal aperture, the actual water level rise of the fractures will be

$$\Delta h' = h - \frac{nbth}{S_{aq} + nbt} \qquad (28)$$

where $\Delta h'$ represents the actual water level rise of each fracture, and h is the nominal water level rise of each fracture. The water level of the aquifer exposed to the atmosphere is reduced by $nbth/(S_{aq} + nbt)$.

According to Eqs. (1), (6), (11) and (28), the final water level of each fracture in the parallel fracture system can be expressed as

$$z = z_0 + \frac{V}{nbt} + \frac{2\sigma \cos\theta(b+t)S_{aq}}{(\rho_w - \rho_n)gbt(S_{aq} + nbt)} \qquad (29)$$

It can be seen that Eqs. (29) and (16) are the same except for the areas of the aquifer and the farctures exposed to the atmosphere. Thus, interconnected fractures can be considered as a whole. When the water level variation of vertical fractures with equal aperture is calculated, the interconnected fractures are calculated as a whole, and the isolated fractures are calculated separately.

2.3 Parallel unequal aperture vertical fractures

2.3.1 Bottom separation condition

The water level change of parallel vertical fractures with equal aperture has been studied above. However, in the realistic situations, the apertures of fractures are rarely the same. Therefore, the research scope is extended to discuss the change of aperture t. It is assumed that aperture t always changes with
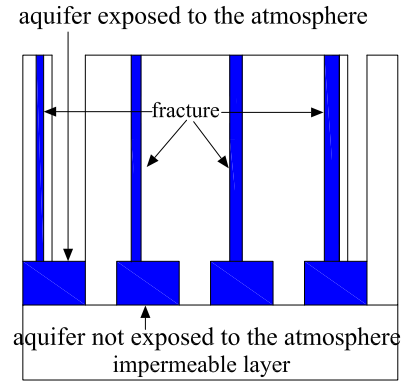

Fig. 7. Parallel and vertical separated fractures with unequal aperture.

the fracture, and the aperture of the ith fracture is expressed as t_i. Due to the assumption that fractures are separated, they do not affect each other. Fig. 7 shows the parallel and vertical separated fractures with unequal apertures.

If the precipitation entering the fracture system is V, then the water level growth Δz caused by precipitation will be

$$\Delta z = \frac{V}{b\sum t_i} \qquad (30)$$

where the value range of i is 1 to n, and n represents the number of fractures in the fracture system. In the first i fracture, the water level increment h_i due to capillary pressure is

$$h_i = \frac{2\sigma \cos\theta(b+t_i)}{(\rho_w - \rho_n)gbt_i} \qquad (31)$$

Considering the decrease of aquifer water level, it can be deduced that

$$\Delta h_i = h_i - \frac{bt_i h_i}{S_{aqi} + bt_i} \qquad (32)$$

where Δh_i represents the actual water level rise of the ith fracture, and S_{aqi} is the area of the aquifer of the ith fracture exposed to the atmosphere.

According to Eqs. (6), (30), (31) and (32) for the whole fracture system, the final water level of each fracture should be

$$z_i = z_0 + \frac{V}{b\sum t_i} + \frac{2\sigma \cos\theta(b+t_i)S_{aqi}}{(\rho_w - \rho_n)gbt_i(S_{aqi} + bt_i)} \qquad (33)$$

The above formula shows that the final water level of a specific fracture changes with its own aperture, whose value is t. That is, z is a function of t. The decisive factor of the final water level is discussed in 2.2.1, and will not be repeated here.

2.3.2 Bottom interconnection condition

Fig. 8 shows the parallel and vertical interconnected fractures with unequal aperture.

Since the fracture system is connected, the equation applicable to the ith connected fracture can be extended similarly to Eqs. (24) and (28):

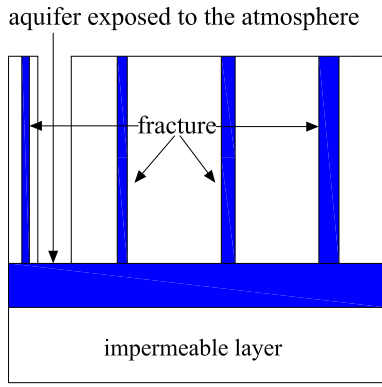$$\Delta h = \frac{b\sum(t_i h_i)}{S_{aq} + b\sum t_i} \qquad (34)$$

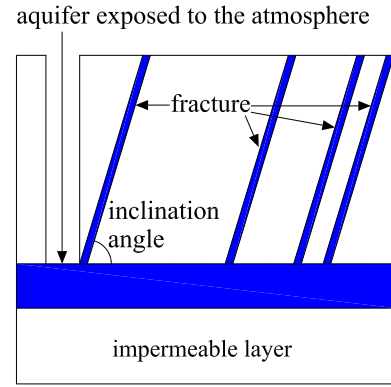**Fig. 8.** Parallel and vertical interconnected fractures with unequal aperture.

Fig. 9. Schematic diagram of distribution of inclined fractures.

$$\Delta h_i = h_i - \frac{b\sum(t_i h_i)}{S_{aq} + b\sum t_i} \tag{35}$$

where Δh_i represents the actual water level rise of each fracture, and h_i is the nominal water level rise of each fracture.

Referring to the h_i of a single fracture under the separation condition, the nominal water level rise under the interconnection condition agrees with that according to Eq. (31).

The water level of the aquifer exposed to air is reduced by $b\sum t_i h_i/(S_{aq} + b\sum t_i)$. According to Eqs. (6), (30), (31) and (35), the final water level z_i of each fracture in the parallel fracture system will be

$$z_i = z_0 + \frac{V}{b\sum t_i} + \frac{2\sigma\cos\theta(b+t_i)S_{aq}}{(\rho_w - \rho_n)gbt_i(S_{aq} + b\sum t_i)} \tag{36}$$

It should be noted that the larger the area of the aquifer exposed to the atmosphere, the higher the final water level of each fracture. In addition, the decrease of fracture aperture also causes the final level of each fracture to increase.

3. Modification and extension of the final water level formula

3.1 Extension of inclination angle

The fracture distribution discussed above is for the vertical situation, which rarely occurs in natural rock and soil masses. Most of the fractures and joints have a certain inclination angle. Therefore, this paper aims to study the effects of fracture distribution on the water level under the inclination condition. All conditions for the vertical fracture system are retained except that the inclination angle is less than 90°. The same conditions for rainfall are also retained, including intensity and distribution. Since the area of the horizontal section of the fracture remains unchanged, it is still expressed as bt, and the amount of water entering the fracture remains V. According to a large number of past studies, the height increment caused by capillary pressure is independent of inclination angle (Cui et al., 2015). Fig. 9 shows the distribution of inclined fractures, while Fig. 10 presents an alternative distribution of inclined fractures. Therefore, the final water level satisfies Eq. (16).
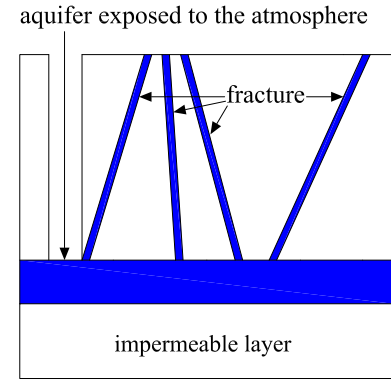

Fig. 10. Alternative distribution of inclined fractures.

The final water level under this condition is equal to that under the vertical condition, and the inclination angle will not affect the final water level of the fracture system. This principle is also applicable to parallel non-uniform aperture fractures, which can be derived by Eq. (33).

Under the interconnection condition, Eqs. (29) and (36) are also applicable to the equal aperture and the unequal aperture conditions.

3.2 Correction of incoming water

The influence of water inflow into the fracture system on water level under a uniform and identical rainfall model has already been discussed (Wang et al., 2021). However, the factors affecting water inflow have not been investigated fully. In China, rainfall intensity is defined as the volume of precipitation per unit area per hour (mm/h) or as the depth of precipitation within 12 or 24 hours. It is assumed that, at a given intensity, the rainfall will be the same at different locations, in other words, the water level increment will the same. In the falling process, however, rainwater will touch the inner surface of the fracture. Due to the effect of friction and surface tension, rainwater will stay on the inner surface, resulting in residual water. Therefore, the actual amount of water to enter the fracture and raise the water level will be smaller than the theoretical value discussed above.

Assuming that water droplets are spherical, when they

approach the inner surface of the fracture and reach a critical distance, water will be adsorbed to the inner surface and eventually settle in the form of continuous film. The shape of water film is toroidal cylinder, while the interface of water-gas phase is cylindrical. Thus, the water film may not cover all of the inner surface. If time is not long enough and the rainfall is only light, water close to the inner fracture surface will be insufficient to cover the whole surface. The size of toroidal cylinder is not only related to rainfall intensity and rainfall time, but also to the shape, mass and movement speed of raindrops, the roughness of fracture inner surface, wettability, and other factors. Specific situations will be analyzed in detail. At present, it is difficult to give a definite unified numerical relation expression for naturally occurring scenarios, thus the effect of these factors can only be studied in an ideal model. It is assumed that all raindrops are spherical with the same size and mass, and that the mass of the raindrops is too small to enable them to split. Raindrops are adsorbed to the inner fracture surface when reach the critical distance d (the vertical distance between the center of gravity and the inner surface), which is generally less than the radius of the raindrop. Rain falls in a uniform distribution. That is, the center of gravity appears in each position with the same probability, and the reference domain is the rectangular of width b and aperture t. Fig. 11 illustrates the rainfall distribution range in a single fracture, where droplets are not absorbed into the inner surface of the fracture.

According to the geometric models of probability, it can be derived that

$$P = \frac{(b-2d)(t-2d)}{bt} \tag{37}$$

where P represents the probability that rainwater will enter the fracture, but cannot be adsorbed to the inner surface, and d is the critical distance. The rainfall intensity is defined as

$$Q = \frac{H}{\Delta T'} = \frac{V'}{S\Delta T'} \tag{38}$$

where Q represents the rainfall intensity, H represents the rainfall accumulation height, $\Delta T'$ represents the time interval, V' represents the volume of rainfall, and S represents the calculated area.

For this case, rainfall intensity can be rewritten as

$$Q = \frac{V'}{bt\Delta T'} \tag{39}$$

The above-mentioned rainfall model agrees with the uniform distribution, therefore the mathematical expectation is

$$E(Q) = \frac{(b-2d)(t-2d)}{bt}Q \tag{40}$$

where $E(Q)$ denotes the mean value of the amount of water that is not adsorbed to the rectangular domain, and Q is the rainfall intensity.
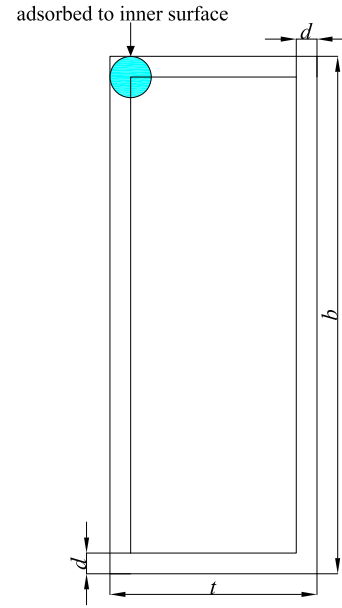

Fig. 11. Rainfall distribution range.

The above equation describes that, with the rainfall intensity $(b-2d)(t-2d)Q/bt$. For parallel isopachous fractures, this can be further obtained as follows

$$V'' = (b-2d)(t-2d)Q\Delta T \tag{41}$$

where V'' indicates the effective inflow volume of a single fracture, and ΔT represents the time interval between water level changes.

By substituting Eq. (41) into Eq. (16), it can be derived that

$$z = z_0 + \frac{P_{aqi}S_{aqi} + (b-2d)(t-2d)}{S_{aqi} + bt}Q\Delta T \\ + \frac{2\sigma\cos\theta(b+t)S_{aqi}}{(\rho_w - \rho_n)gbt(S_{aqi} + bt)} \tag{42}$$

where P_{aqi} represents the probability that rainwater will enter the ith aquifer. As for the parallel and unequal aperture separated fractures, it is deduced that

$$V''' = (b-2d)Q\Delta T(t_i - 2d) \tag{43}$$

where V''' represents the effective inflow volume of a single fracture, and ΔT represents the time interval between water level changes.

The substitution of Eq. (43) into V mentioned in Eq. (33) leads to the following equation:

$$z_i = z_0 + \frac{P_{aqi}S_{aqi} + (b-2d)(t_i - 2d)}{S_{aqi} + bt_i}Q\Delta T \\ + \frac{2\sigma\cos\theta(b+t_i)S_{aqi}}{(\rho_w - \rho_n)gbt_i(S_{aqi} + bt_i)} \tag{44}$$
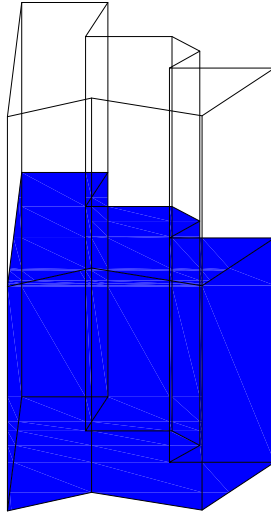
Fig. 12. A cylindrical fracture with an arbitrarily shaped cross-section.

The final water levels in fractures with equal aperture or unequal aperture under the interconnection conditions can be obtained as follows

$$z = z_0 + \frac{P_{aq}S_{aq} + n(b-2d)(t-2d)}{S_{aq} + nbt}Q\Delta T$$
$$+ \frac{2\sigma\cos\theta(b+t)S_{aq}}{(\rho_w - \rho_n)gbt(S_{aq} + nbt)} \tag{45}$$

$$z_i = z_0 + \frac{P_{aq}S_{aq} + (b-2d)\sum(t_i - 2d)}{S_{aq} + b\sum t_i}Q\Delta T$$
$$+ \frac{2\sigma\cos\theta(b+t_i)S_{aq}}{(\rho_w - \rho_n)gbt_i(S_{aq} + b\sum t_i)} \tag{46}$$

where P_{aq} represents the probability that rainwater will enter the aquifer.

From the above formula, it can be seen that the horizontal section shape of the fracture has an effect on the effective water inflow.

3.3 Extension to fracture space

In the aforementioned Eq. (11), which is derived from Eq. (10), the unit of $(b+t)$ is the length unit, while the unit of bt is the area unit, and they represent two physical quantities of perimeter and area, respectively. The question is whether the final formula will still be involved in these two physical quantities if the shape of the section is changed. The fracture space is extended from a quadrangular prism (cuboid) to any column. The column can be a cylinder, a triangular prism, a hexagonal prism, or even a cylinder with an arbitrarily shaped section. Fig. 12 shows the shape of the cylindrical fracture, which has an arbitrary cross-section.

From this point, this research is no longer limited to a fracture with parallel surface. In such fracture spaces, the water-air interface is assumed to be an arc surface, which is subject to surface tension σ, with a wetting angle θ, and that is isotropic. Regardless of the water-air cylinder interface, the vertical component of surface tension on the water-gas

spherical interface is $\sigma\cos\theta$, and the arc integral is performed around the horizontal section:

$$F = \oint \sigma\cos\theta ds \tag{47}$$

which, through calculation, can be expressed as

$$F = \sigma C\cos\theta \tag{48}$$

where F represents the capillary force, and C represents the circumference of the horizontal section.

As the liquid level rises, the water phase invades the gas phase, and the total gravity change in the fracture is expressed as

$$\Delta G = (\rho_w - \rho_n)gSh \tag{49}$$

According to Newton's first law, the following equation can be obtained:

$$\sigma C\cos\theta = (\rho_w - \rho_n)gSh \tag{50}$$

Transposing this equation yields the formula

$$h = \frac{\sigma\cos\theta C}{(\rho_w - \rho_n)gS} \tag{51}$$

When the surface tension, wetting angle, densities of the two phases and the gravitational acceleration are the same, the smaller the ratio of area perimeter, the less the water level rises. In other words, as capillarity is less effective, according to geometric knowledge, given the same circumference, the area of a circle will be the largest. In this case, the water level will rise the least. Therefore, the capillary effects can be alleviated through a circular pore.

It can be seen that Eq. (11) is a special case of Eq. (51). Next, the water inflow is corrected. The water inflow reduction factor of a cylindrical fracture is assumed to be

$$U = \frac{S'}{S} \tag{52}$$

where S' indicates the total area of the center of gravity distribution outside the critical distance of raindrops, and S represents the total area of the horizontal section. Thus, the final water level in the fracture space of a congruent cylinder will be

$$z = z_0 + UQ\Delta T + \frac{\sigma\cos\theta CS_{aq}}{(\rho_w - \rho_n)gS(S_{aq} + S)} \tag{53}$$

and the final water level in the fracture space of similar cylinders will be

$$z_i = z_0 + UQ\Delta T + \frac{\sigma\cos\theta C_iS_{aq}}{(\rho_w - \rho_n)gS_i(S_{aq} + S)} \tag{54}$$

where C_i represents the circumference of the cross-section of similar cylindrical fracture spaces, and S_i is the area of the cross-section. Under the conditions of congruent interconnection, similar separation, and similar interconnection, the final water level is expressed as follows

$$z = z_0 + UQ\Delta T + \frac{\sigma\cos\theta CS_{aq}}{(\rho_w - \rho_n)gS(S_{aq} + nS)} \tag{55}$$

$$z_i = z_0 + UQ\Delta T + \frac{\sigma \cos \theta C_i S_{aqi}}{(\rho_w - \rho_n)gS_i(S_{aqi} + \sum S_i)} \quad (56)$$

$$z_i = z_0 + UQ\triangle T + \frac{\sigma \cos \theta C_i S_{aq}}{(\rho_w - \rho_n)gS_i(S_{aq} + \sum S_i)} \quad (57)$$

3.4 Extension to exhaust conditions

The conditions discussed above are based on the premise that fractures are large enough for water droplets to reach their bottom. If fractures are too narrow, water converges in a small cross-section, making the longitudinal length of the liquid phase larger. Under the action of capillary pressure, gravity, and internal and external air pressure, the flexural rigidity of the liquid phase will then be greater than that of the liquid phase with a larger cross-section. For this reason, water will not easily reach the bottom. Let us suppose that the fractures are narrow enough so that water droplets cannot reach their bottom and displace the gas. They gather together instead, standing in the way between the gas in the fracture and the atmosphere outside. At last, they settle in an equilibrium position. Fig. 13 shows the situation of one droplet balanced in the fracture.

In this case, the capillary pressures at the top and bottom of the liquid column are equal in value, but opposite in direction. The liquid column is subjected to both gravity and total air pressure differences. When the liquid column finally reaches the equilibrium position, the following equation can be obtained:

$$G_1 + p_0 S = p_1 S \quad (58)$$

where G_1 represents the gravity of the liquid column, p_0 is the atmospheric pressure on the top of the liquid column, p_1 represents the air pressure on the bottom of the liquid column, and S is the cross-section area of the fracture. Based on Eq. (46), it can be derived that

$$p_1 = \frac{G_1}{S} + p_0 \quad (59)$$

Assume that the gas in the fracture is an ideal gas and obeys the Ideal Gas Law (Abolpour and Shamsoddini, 2018)

$$pV = \gamma RT \quad (60)$$

where p is the pressure of the ideal gas, V denotes the volume, represents the amount of substance, R is the universal gas constant, γ and T denotes the thermodynamic temperature. The situation is consistent with Boyle's law (West, 1999), and depends on the constant temperature:

$$pV = C \quad (61)$$

where C represents the constant. This process is called isothermal change, and can be obtained as
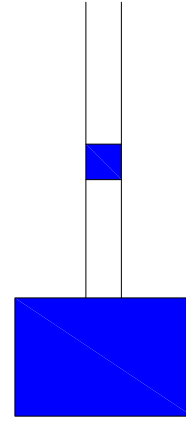
$$p_0 V_0 = p_1 V_1' \quad (62)$$

Fig. 13. Single liquid column condition without air exhaust.

where V_0 is the initial volume of the air column, and V_1 is the volume of the air under the liquid column. The volume of air under the liquid column is as follows

$$V_1' = l_1 bt \quad (63)$$

where l_1 indicates the air height below the liquid column. According to the previous hypothesis, the three edges of the fracture space are l, b and t respectively. The initial air length is l_0, and it can be derived that

$$V_0 = l_0 bt \quad (64)$$

By substituting Eqs. (63), (64) and (59) into (62), the following can be obtained:

$$p_0 l_0 bt = \left(\frac{G_1}{S} + p_0\right) l_1 bt \quad (65)$$

which can be simplified into

$$l_1 = \frac{l_0 S p_0}{G_1 + S p_0} \quad (66)$$

Due to the connection between the aquifer and the atmosphere, when water droplets enter the fracture, the original water level in the fracture will decrease. As determined through analysis, the height difference between the bottom position of the lowest confined space and the water level of the aquifer in the final equilibrium position is V_1/bt. The falling height of gas in the confined space is not equal to the height increase of the aquifer, and satisfies the following formula:

$$\frac{V_1}{bt} = \Delta h \left(1 + \frac{S}{S_{aq}}\right) \quad (67)$$

where Δh represents the falling height of gas in the confined space, and S_{aq} represents the area of the aquifer (excluding the fracture). It can be obtained that

$$\Delta h = \frac{V_1 S_{aq}}{(S_{aq} + S)bt} = \frac{V_1 S_{aq}}{(S_{aq} + bt)bt} \quad (68)$$

Assuming that the volume of the water droplets entering the fracture is V_1, the length of the air column above the liquid column is l'_2, which satisfies the following equation:

$$l'_2 = \frac{l_0 G_1}{G_1 + S p_0} - \frac{V_1}{S} + \Delta h \quad (69)$$

Replacing S by bt, and substituting Eq. (68) into Eq. (69) yields

$$l'_2 = \frac{l_0 G_1}{G_1 + bt p_0} - \frac{V_1}{bt + S_{aq}} \quad (70)$$

The top surface height z_1 of the liquid column is

$$z_1 = z_0 + \frac{l_0 bt p_0}{G_1 + bt p_0} + \frac{V_1}{bt} - \frac{V_1 S_{aq}}{(S_{aq} + bt) bt} \quad (71)$$

where z_0 is the initial level of the fissure water after capillarity occurs. The simplification can be obtained as follows

$$z_1 = z_0 + \frac{l_0 bt p_0}{G_1 + bt p_0} + \frac{V_1}{bt + S_{aq}} \quad (72)$$

It can be seen from the above formula that the water level rise caused by a single droplet entering the fracture is related to the gravity, volume and cross-section area of the fracture, as well as the aquifer area. The expression $V_1/(bt + S_{aq})$ can be regarded as the equivalent water level rise after a raindrop enters the fracture.

Assuming that the second water droplet enters the fracture, the air height can be calculated by using the same method:

$$l_2 = \frac{l'_2 S p_0}{G_2 + S p_0} \quad (73)$$

where G_2 represents the gravity of the second water droplet. By substituting Eq. (70) into Eq. (73), the following equation is obtained:

$$l_2 = \frac{l_0 S p_0 G_1}{(G_2 + S p_0)(G_1 + bt p_0)} - \frac{V_1 S p_0}{(G_2 + S p_0)(bt + S_{aq})} \quad (74)$$

by substituting bt into S, it can be derived that

$$l_2 = \frac{l_0 bt p_0 G_1}{(G_2 + bt p_0)(G_1 + bt p_0)} - \frac{V_1 bt p_0}{(G_2 + bt p_0)(bt + S_{aq})} \quad (75)$$

due to the entry of the second water droplet, the volume of gas in the lowest of confined spaces gets compressed, and the final air column length will be

$$l_{1,2} = \frac{l_0 bt p_0}{G_1 + G_2 + bt p_0} \quad (76)$$

in the above formula, $l_{1,2}$ represents the length of the first confined space after the second water droplet has entered the fracture.
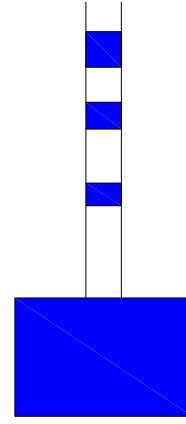

Fig. 14. Multi-liquid column condition without air exhaust.

The length of the air column above the second liquid column is

$$\begin{aligned} l'_3 &= l_0 - l_{1,2} - l_2 - \frac{V_1}{bt + S_{aq}} - \frac{V_2}{bt + S_{aq}} \\ &= \frac{l_0 G_2}{G_2 + bt p_0} - \frac{l_0 bt p_0}{G_1 + G_2 + bt p_0} - \frac{V_1 + V_2}{bt + S_{aq}} \\ &+ \frac{l_0 (bt p_0)^2}{(G_2 + bt p_0)(G_1 + bt p_0)} + \frac{V_1 bt p_0}{(G_2 + bt p_0)(bt + S_{aq})} \end{aligned} \quad (77)$$

The height z_2 of the top surface of the second liquid column is

$$\begin{aligned} z_2 &= z_0 + \frac{l_0 bt p_0}{G_1 + G_2 + bt p_0} + \frac{V_1 + V_2}{bt + S_{aq}} \\ &+ \frac{l_0 bt p_0 G_1}{(G_2 + bt p_0)(G_1 + bt p_0)} - \frac{V_1 bt p_0}{(G_2 + bt p_0)(bt + S_{aq})} \end{aligned} \quad (78)$$

Similarly, the third, fourth and n^{th} water droplet may enter the fracture. Fig. 14 shows the situation of multiple droplets balanced in the fracture.

This scenario satisfies the following equations:

$$l_n = \frac{l'_n bt p_0}{G_n + bt p_0} \quad (79)$$

$$\begin{aligned} l'_n &= l_0 - l_{1,n} + l_{2,n} + l_{3,n} + \ldots + l_{n-2,n-1} + l_{n-1} \\ &- \frac{V_1 + V_2 + \ldots + V_{n-1}}{bt + S_{aq}} \end{aligned} \quad (80)$$

$$l_{i,n} = \frac{l'_i bt p_0}{G_1 + G_2 + G_3 + \ldots G_n + bt p_0} \quad (81)$$

$$\begin{aligned} z_n &= z_0 + l_{1,n} + l_{2,n} + l_{3,n} + \ldots + l_{n-2,n-1} + l_{n-1} \\ &- \frac{V_1 + V_2 + \ldots + V_{n-1}}{bt + S_{aq}} \end{aligned} \quad (82)$$

where l_n represents the length of the nth air column after the nth liquid droplet has entered the fracture; l'_n represents the length of the rest air column in the fracture space before the

n^{th} liquid droplet has entered the fracture; and $l_{i,n}$ represents the length of the ith air column after the nth liquid droplet has entered the fracture. It is important to note that ln in nature is the same as $l_{n,n}$ in nature. The variable z_n is the water level after the nth droplet has entered the fracture, and z_0 denotes the initial water level. When the water level z_n exceeds the highest position $z_0 + l_0$ of the fracture, water overflows and the final water level stays at $z_0 + l_0$. Therefore, the applicable condition of Eqs. (79), (80), (81) and (82) is $z_n \leqslant z_0 + l_0$.

4. Conclusions

In this work, the parallel fractures of rock and soil mass were discussed. The interconnected fractures were calculated as a whole, while the isolated fractures were calculated separately. Results showed that the final water level in parallel fractures is related to the initial water level, rainfall intensity, rainfall distribution, the shape, mass and motion velocity of the incoming raindrop, the geometric characteristics (shape and size) of the horizontal section of the fracture, the wettability of the fracture, and temperature. When the fracture space is a cylinder, the larger the ratio of perimeter to the horizontal section area, the higher the capillary pressure will be, resulting in a more obvious capillary phenomenon. Moreover, the corresponding rainfall reduction coefficient is affected by the shape of the horizontal section. Multiple water droplets may enter the small fracture space. Under the condition of no air exhaust, this scenario can be expressed by the iterative relation, and the water level cannot exceed the highest position of the fracture.

Nomenclature

z = water level
z_0 = initial water level
V = volume of water
b = width
l = length
p_c = capillary force
ΔG = gravity increment
ρ_n = non-wetting phase density
h = water head
σ = surface tension
S_{aq} = area of aquifer exposed to the air
Δh_i = actual water level increment of the ith fracture
d = critical distance
Q = rainfall intensity
$\Delta T'$ = rainfall time interval
$E(Q)$ = mean value of the amount of water
P_{aq} = probability that rainwater will enter the aquifer
P_{aqi} = probability that rainwater will enter the ith aquifer.
ΔT = time interval between water level changes
T = thermodynamic temperature
S = area of the horizontal section
S_i = area of the cross-section of cylindrical fracture spaces
p_0 = atmospheric pressure
R = universal gas constant
Δz = water level variation
$\Delta h'$ = actual height increment

n = number of fractures
t = aperture
R_1, R_2 = curvature radii
F = force
ρ_w = wetting phase density
g = gravitational acceleration
t_i = aperture of the ith fracture
Δh = water head variation
S_{agi} = area of the ith aquifer exposed to the air
h_i = water head of the ith fracture
θ = wetting angle
H = rainfall accumulation height
V' = volume of rainfall
V'' = effective inflow volume
V''' = total effective inflow volume of the fracture system
U = water inflow reduction factor
S' = total area of the center of gravity distribution outside the critical distance of raindrops
C_i = circumference of the cross-section of cylindrical fracture spaces
z_i = water level of the ith fracture
γ = amount of substance
l_0 = initial length of the air column
V_0 = initial volume of the air column
$l_{i,n}$ = length of the ith air column
G_n = gravity of the nth water droplet
l'_n = length of the rest air column
l_n = length of the nth air column

Conflict of interest

The authors declare no competing interest.

References

Abolpour, B., Shamsoddini, R. A novel scheme for predicting the behaviors of liquid and vapor phases of water using the ideal gas theory. International Journal of Thermodynamics, 2018, 21(3): 174-178.

Anderson, S. A., Sitar, N. Analysis of rainfall-induced debris flow. Journal of Geotechnical Engineering, 1995, 121(7): 544-552.

Brand, E. W. Some thoughts on rainfall induced slope failures. International Journal of Rock Mechanics and Mining Sciences & Geomechanics Abstracts, 1984, 21(3): A108.

Brenner, R. P., Tam, H. K., Brand, E. W. Field stress path simulation of rain-induced slope failure. In: Proceedings of 11th international conference on soil mechanics and foundation engineering, pp. 373–376, 1985.

Cho, S. E. Stability analysis of unsaturated soil slopes considering water-air flow caused by rainfall infiltration.

Engineering Geology, 2016, 211: 184-197.

Cui, Y. Q., Huang, Y., Gao, M. X., et al. Study on the law of motion of water in glass capillary. Science and Technology Innovation Herald, 2015, 12(23): 44-45. (in Chinese)

Dill, H. G. Kaolin: Soil, rock and ore: From the mineral to the magmatic, sedimentary and metamorphic environments. Earth-Science Reviews, 2016, 161: 16-129.

Ding, X., Liang, X., Zhang, Y., et al. Capillary water absorption and micro pore connectivity of concrete with fractal analysis. Crystals, 2020, 10(10): 1-13.

Dong, J. B. LBM simulations and experimental validations of fluid flow through single fractures in rock media. China University of Mining and Technology, PhD, 2020. (in Chinese)

Kristo, C., Rahardjo, H., Satyanaga, A. Effect of variations in rainfall intensity on slope stability in Singapore. International Soil and Water Conservation Research, 2017, 5(4): 258-264.

Liu, H., Cao, G. Effectiveness of the Young-Laplace equation at nanoscale. Scientific Reports, 2016, 6: 23936.

Lu, N., Godt, J. Hillslope Hydrology and Stability. New York, USA, Cambridge University Press, 2013.

Nesbitt, H. W., Young, G. M. Early proterozoic climates and plate motions inferred from major element chemistry of lutites. Nature, 1982, 299(5885): 715-717.

Regmi, R. K., Jung, K., Nakagawa, H., et al. Study on mechanism of retrogressive slope failure using artificial rainfall. Catena, 2014, 122: 27-41.

Regmi, R. K., Jung, K., Nakagawa, H., et al. Numerical analysis of multiple slope failure due to rainfall: Based on laboratory experiments. Catena, 2017, 150: 173-191.

Sasaki, S., Ishiguro, R., Caupin, F., et al. Superfluidity of grain boundaries and supersolid behavior. Science, 2016, 313(5790): 1098-1100.

Sidle, R. C., Swanston, D. N. Analysis of a small debris slide in coastal Alaska. Canadian Geotechnical Journal, 1982, 19(2): 167-174.

Sitar, N., Anderson, S. A., Johnson, K. A. Conditions leading to the initiation of rainfall-induced debris flows. In Stability and Performance of Slopes and Embankments II: Proceedings of a Specialty Conference, American Society of Civil Engineers. Geotechnical Engineering Division, American Society of Civil Engineers, 1992.

Terzaghi, K. Mechanism of landslides, in Application of Geology to Engineering Practice, edited by K. Terzaghi and S. Paige, Berkey Volume, New York, pp. 83-123, 1950.

Wang, E. Z., Wang, H. T., Sun, Y. Study on seepage flow model in double fracture systems. Chinese Journal of Rock Mechanics and Engineering, 1998, 17(4): 400-406. (in Chinese)

Wang, G., Sassa, K. Pore-pressure generation and movement of rainfall-induced landslides: Effects on grain size and fine-particle content. Engineering Geology, 2003, 69(1-2): 109-125.

Wang, L., Li, G., Chen, Y., et al. Field model test on the disaster mechanism of artificial cut slope rainfall in Southern Jiangxi. Rock and Soil Mechanics, 2021, 3: 1-10. (in Chinese)

West, J. B. The original presentation of Boyle's law. Journal of Applied Physiology, 1999, 87(4): 1543-1545.

Zheng, Z. C., Liu, Y., Wang, M., et al. Experiments and model on contaminant transport in a single marble parallel plate fracture using continuous time random walk. Journal of Hefei University of Technology (Natural Science), 2019, 42(5): 677-682. (in Chinese)